The International Journal of Advanced Manufacturing Technology (2024) 130:4053–4066
https://doi.org/10.1007/s00170-024-12949-6

ORIGINAL ARTICLE

The effect of surface finish and post-processing on mechanical properties of 17-4 PH stainless steel produced by the atomic diffusion additive manufacturing process (ADAM)

Tahsin Tecelli Opoz[1] · Andrew Burgess[1] · Juan Ignacio Ahuir-Torres[1] · Hiren Ramniklal Kotadia[1,2] · Samuel Tammas-Williams[3]

Received: 31 July 2023 / Accepted: 1 January 2024 / Published online: 12 January 2024

Abstract
This study investigates the influence of surface finish and post-processing conditions on the mechanical properties of 17-4 PH stainless steel (SS) produced using the atomic diffusion additive manufacturing process (ADAM). Diverse sample orientations, including horizontal (0°), 30°, 60°, and vertical (90°), were examined, with selected samples undergoing post-processing through machining, polishing, and heat treatment. Tensile strength testing, surface roughness measurement, and hardness measurement were conducted to assess the effect of surface finish conditions and post-processing on mechanical properties. The results reveal significant variations in the tensile strength of the samples based on the build orientation (183.5 to 1034.5 MPa), and subsequent machining. Notably, post-built machining is found to enhance both the absolute ultimate tensile strength (UTS) and the isotropy of the material. Further improvements are attainable through heat treatment. A microstructure analysis, in conjunction with tensile testing outcomes, demonstrates the potential for refining the properties of ADAM-printed samples through suitable machining, heat treatment, and geometry modifications. This study identifies avenues for ongoing process development and outlines possibilities for enhancing mechanical properties of additive manufactured parts, particularly through ADAM process.

Keywords Additive manufacturing · 17-4PH stainless steel · Tensile testing · Surface roughness · Defects

1 Introduction

Additive manufacturing (AM) or 3D printing technology can print unique metallic parts that cannot be fabricated by conventional manufacturing [1]. AM provides various advantages such as creating complex shape components, and significant weight saving with less material waste while maintaining strength and structural integrity [1–5]. Particularly, weight reduction in components used in the automotive and aerospace industries poses challenging design problems. Components aiming for weight reduction often involve complex geometrical structures that necessitate topology optimization and lattice structures. AM is an emerging manufacturing technique capable of producing these intricate structures filled with lattice formations [4]. Currently, AM has been adopted by various industries including aerospace and medical, and to produce machine tools [6]. However, the uptake of metal AM in safety-critical engineering is hindered by many technical challenges such as defects and poor dimensional accuracy [3, 7, 8]. These technical challenges in the AM have led to the development of hybrid manufacturing processes comprising of AM parts followed by post-processing such as machining operations become essential requirement to maintain the desired mechanical property and dimensional accuracy [9, 10].

There are various metal AM technologies developed over the years, including, powder bed fusion (PBF), directed energy deposition (DED), binder jetting (BJ), and ultrasonic additive manufacturing (UAM) [11–13]. The prominent metal AM technology today is the PBF process. One of the key concerns with the PBF process is powder cost,

✉ Tahsin Tecelli Opoz
T.T.Opoz@ljmu.ac.uk

[1] School of Engineering, Liverpool John Moores University, Liverpool L3 3AF, UK

[2] WMG, University of Warwick, Coventry CV4 7AL, UK

[3] School of Engineering, The University of Edinburgh, Edinburgh EH9 3JL, UK

availability of alloy compositions, strict powder handling requirements, recycling, and the challenge of removing powder from components after the building process [3, 14, 15]. Some of the challenges related to powder handling could be explosion risk, occupational health, labour costs, powder recovery, cleaning quality, and process repeatability [16–18]. Furthermore, these techniques require a high initial investment. These challenges and risks pose obstacles that make small businesses hesitant to adopt AM technologies for their metal part production line. However, in response to these difficulties associated with conventional metal AM technologies, the development of metal-based fused filament fabrication (FFF) technology has emerged as a promising solution [19].

Metal FFF is considered more economical and involves negligible powder-related risk and health concerns compared to PBF and DED processes [20]. Metal FFF deposits composite filament feedstock made of metal powder and a polymer binder, similar to that of polymer-type FFF. The metal FFF systems use three different stages to complete the AM process: printing, debinding, and sintering. In the printing stage, a composite filament made of metal powder mixed with thermoplastic polymer, and the binding agent is extruded at a sufficient temperature to melt the composite filament and deposited layer by layer to form the part; the printed part is defined as a 'green part', which is a fragile part, not strong enough to carry any significant loading. The second stage is debinding where the green part is washed in a debinding agent to remove the polymer-binding agent; after the debinding process, the part is called a 'brown part'. The third stage is the sintering process, where the brown part is sintered in a furnace to obtain a compact, nearly fully dense, strong part. During the sintering process, the weakly bonded metal particles fused in a temperature-controlled chamber.

Very few research papers have been published so far regarding the metal FFF process. Two notable metal FFF processes available in the industry include the Atomic Diffusion Additive Manufacturing (ADAM) and Bound Metal Deposition (BMD) methods. In addition to these processes, the BASF 3D Printing Solution GmbH group company has begun supplying metal-based spools of filament designed for use in existing cost-effective FFF printers. BASF currently offers ultrafuse 17-4PH and 316L stainless steel (SS) filaments. For the ADAM process, filament materials include 17-4PH SS, copper, Inconel625, H13 tool steel, A2, and D2 tool steels. On the other hand, filament materials available for the BMD process encompass 17-4PH and 316L SS, copper, D2 tool steel, H13 tool steel, Inconel 625, and Titanium Ti64.

Most of the researchers have investigated the dimensional accuracy of printed parts [21, 22], the mechanical property of parts built with differing orientations [16, 21, 23–25], and microstructural and porosity analysis of the printed parts [21, 23, 26, 27]. Gonzalez-Gutierrez et al. [28] conducted a comprehensive review on various extrusion-based AM processes, including FFF, ADAM, and BMD. Although these processes may have different names due to patented technologies and commercialisation by different companies, they share a similar material deposition mechanism. For instance, Stratasys patented and commercialized the material extrusion of filament as Fused Deposition Modelling (with the trademarked acronym FDM™), but this is essentially the same process as FFF. Parenti et al. [22] focused on defect-free fabrication of gyroid cellular structures using the BMD process, successfully producing single-cell gyroids with thicknesses exceeding 1 mm and relative densities above 20%. Jiang and Ning [27] investigated the relationship between process, microstructure, and performance for lattice structures made of 17-4PH SS using the ADAM process. Their study revealed that the sintered specimens exhibited equiaxed grain morphology, consisting mainly of austenite phases with some observed martensitic phases on the top surface. Compression testing on different lattice structures demonstrated that the BCC-FCC lattice had the lowest mechanical performance due to higher defects compared to the other lattice structures. Jian and Ning [27] also examined the tensile and flexural fatigue strength behaviour of ultrafuse 316L-built samples, providing insights into the impact of the printing process and microstructure on the fatigue properties of metal parts. Pellegrini et al. [25] investigated the anisotropic mechanical behaviour of FFF-printed ultrafuse 316L parts through tensile testing coupled with digital image correlation (DIC) and finite element analysis (FEA). Flat dog-bone test specimens were built in three different orientations denoted upright (aligned with the build direction), flatwise (flat on the build plate), and sideways (narrow edge on the build plate) with varying numbers of wall layers. The upright specimens exhibited the lowest UTS, while the flatwise and sideways specimens showed greater tensile strength. Increasing the number of wall layers consistently decreased Poisson's ratio, especially in the upright specimens, while flatwise and sideways samples exhibited a nearly constant Poisson's ratio. Lavecchia et al. [25] compared the mechanical performance and microstructure of 17-4PH SS samples fabricated using two technologies: ADAM and FFF with ultrafuse filament. Their investigation revealed significant differences in tensile strength, porosity, and microstructure formation due to variations in sintering and debinding methods. Suwanpreecha et al. [16] reported the mechanical properties of 17-4PH steel fabricated by metal-fused filament fabrication, highlighting the effect of different specimen layouts (flatwise, sideway, and upright) on relative density and mechanical properties. All specimens exhibited high relative density (97 to 98.5%), but flatwise and sideway specimens demonstrated high

repeatability in tensile strength. Galati and Minetola [29] evaluated the dimensional accuracy of parts produced using the ADAM process and found that it achieved an IT13 grade based on ISO IT grades of a reference artefact.

The build orientation and print direction of a three-dimensional part significantly influence various factors, including part quality, waste generation, production time, and cost. Achieving an optimal build orientation is crucial for enhancing the sustainability of the AM process, as it minimises support structure volume and build time [5, 30]. Gunaydin et al. [30] conducted a detailed investigation into the optimization of build orientation and its impact on support structure volume and build time in laser powder bed fusion. It is worth noting that a similar methodology could be applied to FFF type AM processes. Alkindi et al. [31] investigated the influence of print orientations on the tensile strength of parts printed using the ADAM process. They varied the print orientations from 0 to 90° with a 10° increment and found that the upright (90°) printed specimen exhibited an UTS of 440.15 MPa, being less than 50% of the horizontal (0°) printed specimen. Henry et al. [23] conducted a study on the mechanical characterization of 17-4PH SS samples printed using the ADAM process. The printed samples were subjected to various loading conditions, including tensile, shear, and bending. The results indicated that the failure loads for all loading conditions were influenced by the orientation of the printed parts, following a similar trend. Tosto et al. [32] conducted a study on the mechanical characterization of parts printed with 17-4PH steel using the ADAM process and ultrafuse 316L filament using FFF. Specifically, they examined the green parts to identify any defects resulting from filament deposition and their impact on the microstructural integrity and tensile properties of the sintered parts. The defects observed in the green state led to voids and inadequate interlayer bonding during the sintering process, resulting in reduced tensile properties of the sintered parts. Similarly, Leonard and Tammas-Williams [26] used non-destructive X-ray computed tomography to quantify the same defects as-deposited (pre sintering) and after sintering. They found that while significant shrinkage occurred during sintering, this did not lead to any healing of voids. Table 1 summarises a comparison of UTS values for 17-4PH stainless steel manufactured using the ADAM process, as reported in the literature. The UTS values were primarily determined from samples tested in their as-sintered (as-built) condition, without undergoing any post-processing. Notably, the results indicate that samples built horizontally at 0°, specifically alongside the side-face, exhibited the highest UTS values. In contrast, samples built in the vertical direction, or any other orientation demonstrated lower UTS values. For reference, Markforged has reported the UTS values of 17-4PH steel as 1050 MPa in the as-sintered condition [33]. After undergoing an additional heat treatment process known as H900 (482 °C (900 °F) for 1 h), the UTS value is stated to increase to 1250 MPa. However, it is important to note that the datasheet from Markforged does not provide specific information about the build orientation of the samples.

Table 1 Summary of UTS values of 17-4PH SS fabricated by the ADAM process in the literature

Reference	Building orientation	UTS (MPa)
Henry et al. [23]	0° (horizontal) 90° (vertical) 0° (side)	776–795 (as-sintered) 647 (as-sintered) 999 (as-sintered)
Lavecchia et al. [25]	0° (horizontal) 90° (vertical)	858–898 (as-sintered) 472–552 (as-sintered)
Alkindi et al. [31]	0° (horizontal) 30° 60° 90° (vertical)	947.26 (as-sintered) 650 (as-sintered) 418 (as-sintered) 440.15 (as-sintered)
Markforged [33] 17-4 PH SS-v1 material data sheet	Not specified	1050 (as-sintered) 1250 (H900)

It is worth noting that most of the existing research on metal filament AM technologies, such as ADAM, BDM, and ultrafuse metal filament with FFF, has primarily focused on the mechanical characterization of as-built parts, while investigations on post-processed parts are limited and require further exploration. However, most AM parts need post-processing such as machining, polishing, and heat treatment to meet their geometrical and functional requirements. There is a lack of systematic research considering the post-processing requirement of AM parts. The post-processing requirement is considered the 'Achilles heel' that can run up to 60% of the cost of the finished part due to labour-intensive and time-consuming surface finishing activities. The post-processing requirement including the effect of surface finish on the mechanical properties of 3D printed parts has not yet been fully explored. Therefore, in this study, the effect of post-processing methods including surface finish and heat treatment on the mechanical properties of parts built by the ADAM process has been investigated. The main objective of this study is to investigate the impact of different post-processing methods, such as machining, polishing, and heat treatment, on the mechanical properties of 3D- FFF printed parts fabricated using 17-4PH SS alloy. This alloy is widely employed in various industries, including chemical, petrochemical, and metalworking, owing to its remarkable corrosion resistance, high strength, and favourable weldability [34]. The study aims to enhance our understanding of the factors influencing the mechanical properties of 3D printed parts made from 17-4PH SS alloy and provide valuable insights into optimising the manufacturing process to meet the specific requirements of diverse applications.

2 Materials and method

2.1 Materials

The 17-4PH SS in the form of filament supplied by Markforged was used for the 3D printing. The chemical composition (in wt.%) of 17-4PH SS is given in Table 2. The filament is a composite material containing a 60% volume fraction of 17-4PH SS powder, and the remaining binders are made of paraffin wax (20 vol.%) and polythene (20 vol.%) [27].

2.2 ADAM process

The 3D printing ADAM process was carried out using the MetalX^{TM} 3D printer supplied by Markforged. The ADAM process consists of three discrete sequential phases: print, wash, and sinter as shown in Fig. 1. All process stages from print file generation to the sintering phase are controlled by Markforged's cloud-based proprietary software called Eiger. The 3D printing system uses predefined process parameters (e.g., printing speed, extruder temperature, sintering temperature profiles). The Eiger software allows the user to manipulate the orientation of a part, select one of the available infill patterns (solid fill, triangular fill, gyroid fill), and the number of wall layers. In this study, samples were manufactured with four vertical wall extrudes and solid (100% relative density) infill material deposition selected in the Eiger software.

During the 'print' phase, the filament material is heated and extruded onto the build plate, through a twin nozzle system with a diameter of 0.4 mm to produce a 'green' part. The first nozzle extrudes metal filament to build the part, support structure, and raft. The raft is an interface structure between the part and the build plate, which could minimise warpage and securely hold printed parts. The second nozzle is used to dispense a ceramic material between the parts and other structures (raft and support) to ease the removal of these support structures from the part once the full process is completed. The 3D printing system then deposited walls/perimeters around the edge of each layer profile. The internal area was then filled with an alternating infill at +45°/–45° angles. The Eiger software also automatically scales up the designed geometry by 20% to account for the shrinkage during the sintering phase. The subsequent operation is the 'wash' phase (Wash-1 by Markforged), where the parts built in the printing phase will be washed in a debinding solution (Opteon SF 79) to dissolve the polymer binding agent and is considered a 'brown' part in the post-washing phase. The Eiger software estimates the washing time. The washing process finishes when the part losses approximately

Table 2 Composition of 17-4PH stainless steel in wt.% [33]

	Cr	Ni	Cu	Si	Mn	Nb	C	P	S	Fe
Min-max	15–17.5	35%	35%	1	1	0.15 –0.45	0.07	0.04	0.03	Balance

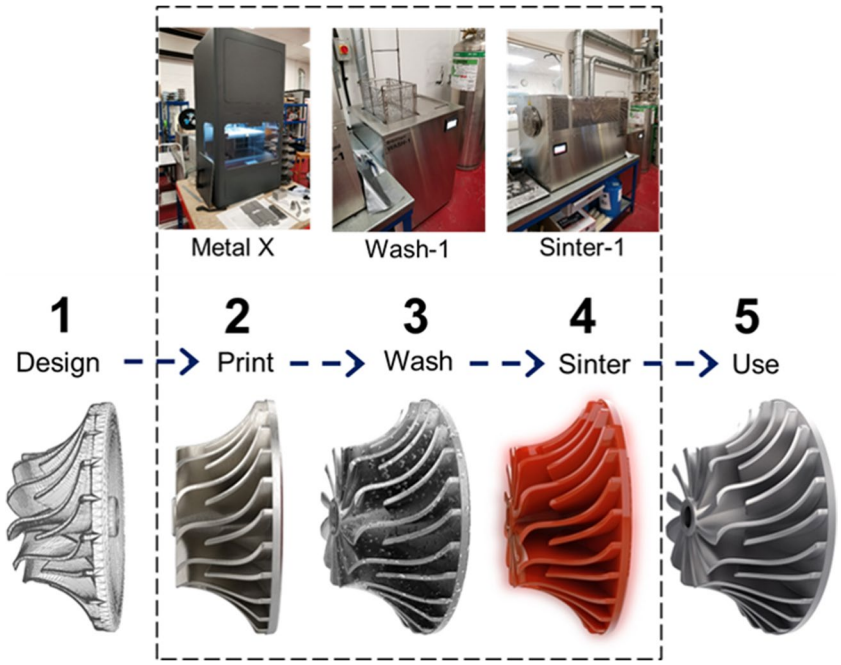

Fig. 1 A diagram illustrating the processing phases in the ADAM process (adapted from Markforged Metal 3D Printer: The Metal X 3D Printing System at https://markforged.com/)

4.1% of the initial weight [25]. During the 'sintering' phase, the components are heated in an industrial furnace (Sinter-1 by Markforged) under an argon atmosphere with 3% hydrogen to prevent oxidation of the material [25], through an initial debinding temperature at which any remaining polymeric binder is burned off, and then to a higher sintering temperature. The actual temperatures used are not revealed during processing and remain the intellectual property of the manufacturer. However, the maximum sintering temperature for 17-4PH stainless steel is estimated to be about 1100 °C [25], while the maximum stated temperature of the furnace is 1300 °C, and it is likely that the temperature profile is based on previously used temperatures for metal injection moulding. The brown components underwent a 27-h sintering process, consistent with the standard procedure for 17-4PH stainless steel, within the furnace (referred to as sinter-1), to complete the manufacturing process. The specific temperature and duration profile for the sintering procedure were not disclosed and remain proprietary information belonging to the manufacturer. Following the atomic diffusion process (i.e. sintering), the metal particles fuse together to form a dense part, while the ceramic supports turn from filament to powder to allow easy release of supports. Thus, leaving the cooled part ready for use or post-processing through techniques such as heat treatment or machining. Throughout this paper, samples are referred to as 'as-built' to indicate they have completed the full 'building' process prescribed by the manufacturer but not been subjected to further heat treatment or surface finishing.

2.3 Experiment setup and post-processing methods

Two different methods were used to fabricate the tensile test specimens: (1) the specimens were produced in their as-built condition without any machining, and (2) post-machining was performed on the as-built cylindrical samples. Figure 2 shows the diagram for the strategy followed for the printing and post-processing of tensile test samples. Samples with different orientation and tensile test specimen dimensions are shown in Fig. 3. Computer-Aided Design (CAD) software (SOLIDWORKS) was used to generate models which were then exported as a stereolithographic (STL) file, suitable for import by the Eiger software. Table 3 summarises the list of experimental conditions. To ensure repeatability, four samples were tested for each condition, amounting to a total of 40 manufactured samples. This approach allowed for conducting multiple measurements to validate the consistency of the results.

At first, the net shape sample was constructed vertically, with supports included to accommodate the overhanging grip section (Fig. 4a). However, the removal of these supports without causing damage to the gauge length proved to be impractical. The decision was made to not tensile test these specimen, but they were used for hardness evaluation. Consequently, a slight modification was made to the geometry, replacing the filleted edge at both ends of the gauge length with a 60° chamfer. The modified geometry is illustrated in Fig. 4b. With this adjustment, the sample geometry allowed for fitting into the tensile testing rig without requiring additional supports during printing. The samples featuring the adapted geometry are denoted with an asterisk ('*') in Table 3, along with their corresponding test results. It is

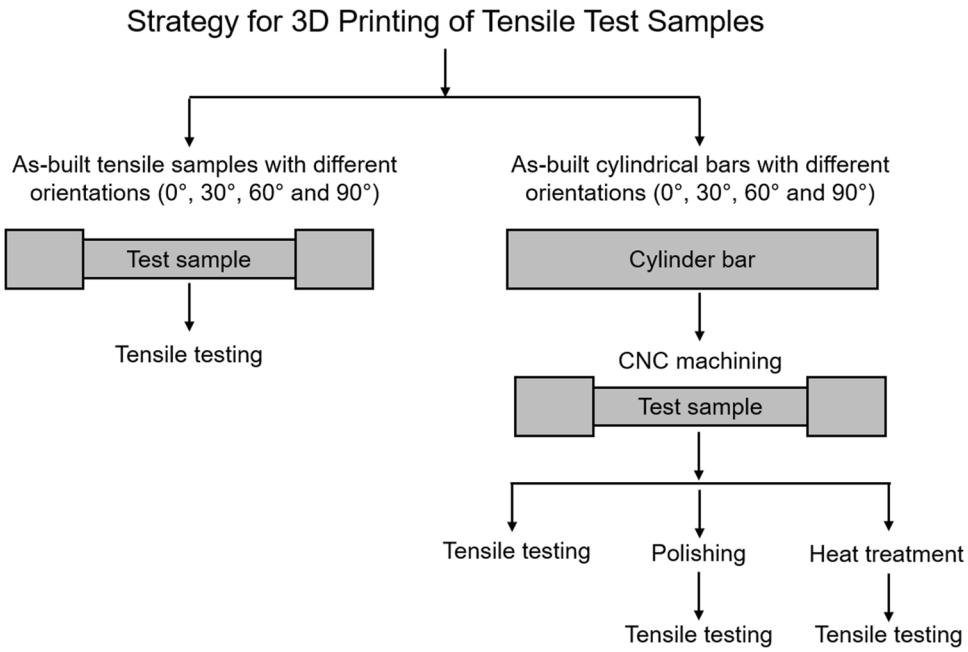

Fig. 2 Flow chart showing design of experiments with as built and post-processing before the tensile testing

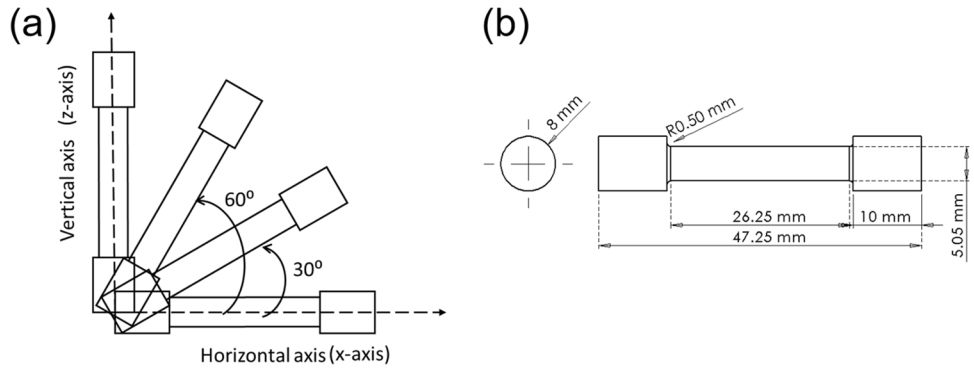

Fig. 3 Tensile cylindrical samples. **a** Orientation from horizontal (0°) to vertical (90°) and **b** dimensions

Table 3 List of conditions tested

Initial geometry	Orientation	Machined	Polished	Heat treated
Net shape	0° (horizontal)	No	No	No
Net shape	30°	No	No	No
Net shape	60°	No	No	No
Net shape*	90° (vertical)	No	No	No
Cylinder	0° (horizontal)	Yes	No	No
Cylinder	30°	Yes	No	No
Cylinder	60°	Yes	No	No
Cylinder	90° (vertical)	Yes	No	No
Cylinder	90° (vertical)	Yes	Yes	No
Cylinder	90° (vertical)	Yes	No	Yes

*Defines the modified geometry (see Fig. 4b)

Note that for each condition, four samples were tested and 40 samples were built in total

expected that this change will have minimal impact on the results, as the gauge length section of the sample remained consistent. However, it is important to acknowledge that this sample underwent a separate sintering cycle compared to the other specimens.

A computer numerical control (CNC) lathe, specifically the XYZ Machine Tools PROTURN SLX 355, was utilised for machining the cylindrical specimens. To improve the surface finish of one group of specimens, an OTEC EF18 Mass Finisher was utilised. During this process, plastic conical chips were rotated at 310 RPM for 2 h while the specimens were submerged within them. Meanwhile, another group of specimens underwent a H900 heat treatment process at 482.2 °C (900 °F) for 1 h in Omegalux LMF-3550 programmable furnace, followed by air cooling. A surface roughness measurement instrument (Taylor-Hobson Form Talysurf i-Series) was used to measure the surface profile of the net-shaped, machined, and polished sample along the longitudinal direction of the samples, and the Taylor Hobson software (Ultra) was used to determine the average surface roughness (R_a) value for each condition. 3D surface profiles and macrostructure of the samples were also captured via Keyence VHX series Digital Microscope.

2.4 Mechanical testing

Uniaxial tensile testing was conducted following the ASTM E8 standard, employing a Tinius Olsen H50 KS tensile testing machine with a constant extension rate of 5 mm/min. The small size of the specimens precluded the use of a strain gauge, but the extension was recorded and used to calculate

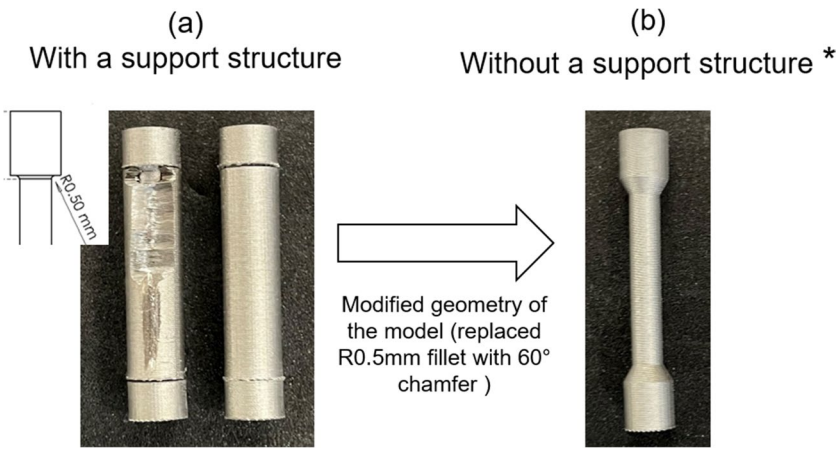

Fig. 4 Example of samples built with a vertical (90°) orientation. **a** With a support structure. **b** With modified geometry without a support structure

the sample strain after correcting for the testing machine compliance.

Hardness tests were conducted employing the Mitutoyo HR-400 series under Rockwell Hardness C test conditions specified for 17-4PH stainless steel, utilising a diamond indenter at a load of 150N along the cross-section of the tensile specimen. As the hardness test was performed on the internal geometry of the part, the influence of machining and polishing can be neglected.

2.5 Microstructure and fracture surface analysis

Samples were examined after tensile testing using both optical and scanning electron microscopy (SEM). For microstructure imaging, a surface normal to the testing direction in the grip ends of the specimen was prepared to a mirror finish by using standard metallography techniques. An FEI Inspect S50 SEM equipped with energy dispersive x-ray spectroscopy (EDS) was used for fractography, high resolution qualitative pore analysis, and chemical analysis of inclusions. An accelerating voltage of 20 kV and a current of 16 nA was used. Images were segmented into solid and void using the default automatic threshold level in Image-J before quantification. Also, the Archimedean method was employed to conduct density analysis in accordance with the ASTM B962-17 standard, with each sample being measured three times.

3 Results

The mechanical and surface finish properties of the ADAM-processed samples were compared to understand the impact of build orientation and post-processing on their mechanical performance. Additionally, the fracture surfaces using SEM with EDS analysis were examined to gain insights into the factors contributing to mechanical performance.

3.1 Mechanical properties

Typical results of the tensile testing, shown in Fig. 5, indicate that the samples exhibit limited plastic deformation, with failure occurring shortly after reaching the elastic limit with minimal plastic deformation. This suggests that the material has low ductility, and from here, UTS alone is used to quantify the tensile properties of the material. The variation in UTS, considering the impact of post-processing techniques such as machining, polishing, and heat treatment, is shown in Fig. 6.

Analysis of the impact of build orientation on the UTS of the as-built samples reveals significant anisotropy, as depicted in Fig. 6a. Based on the average results obtained from four samples, the samples built with a 0° orientation

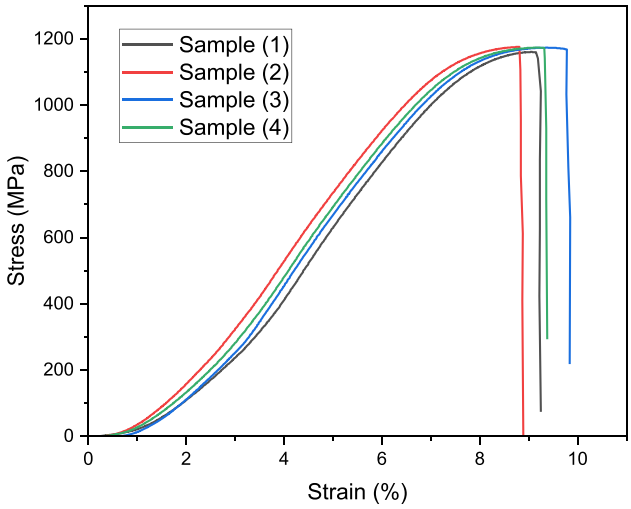

Fig. 5 Example stress-strain curves for the horizontal (0°) samples after machining demonstrates test repeatability and limited ductility

(horizontal) exhibit the highest UTS at 1034.5 MPa. On the other hand, the samples built with a 60° orientation exhibit a noticeably lower UTS at 183.5 MPa. Overall, the results suggest that samples printed between horizontal (0°) and vertical (90°) orientations exhibit lower UTS values compared to samples printed at 0° or 90° orientations.

Fig. 6b provides a comparison of the impact of various post-processing techniques (machining, polishing, and heat treatment) on the UTS of the printed samples. The average surface roughness (R_a) values are also included. R_a values were extracted using the Talysurf stylus along the longitudinal direction of the samples, which coincides with the direction of tensile loading. The as-built samples, which have higher surface roughness, demonstrate lower UTS values compared to the post-machined, polished, and heat-treated with post-machined samples, which exhibit lower surface roughness values. Notably, the heat-treated (H900) samples combined with post-machining, display the highest UTS value among the different post-processing techniques.

After machining, the horizontally printed samples (0° orientation) again exhibited the highest UTS value with an average of 1171.2 MPa (Fig 6c). The UTS values of samples with 30°, 60°, and 90° built orientations were similar after post-machining, averaging around 1000 MPa.

The relationship between the Rockwell hardness (HRC) of different samples obtained from various orientations, including both as built and post-processed samples is shown in Fig 6d. The results demonstrate that the hardness of most samples is relatively consistent, averaging around 30 HRC. However, the heat-treated samples and the modified geometry vertically as-built samples both showed a hardness of approximately 36 HRC. The H900 heat treatment is expected to increase the hardness. However, the

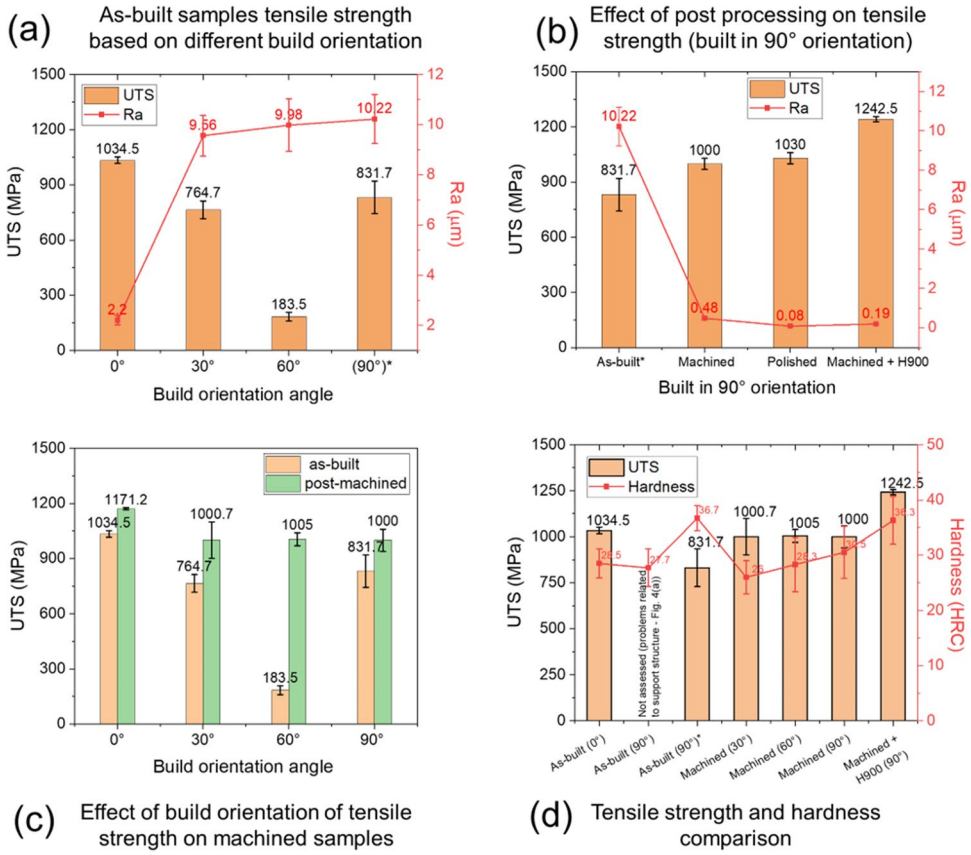

Fig. 6 Illustration of the variation of UTS and hardness across different build orientations and post-processing conditions. **a** Depiction of UTS and surface roughness (Ra) in relation to build orientation. **b** A display of UTS and Ra concerning various post-processing techniques applied to vertically built samples. **c** Comparison of UTS values between as-built and machined samples at different orientations. **d** Presentation of UTS and Hardness (HRC) with respect to different post-processing methods and orientations. Error bars represent the standard deviation of four measurements

reason for the increased hardness in the modified vertical geometry is less clear, especially when both the original geometry vertical sample and machined vertical sample had a very similar hardness to all other orientations. It is worth noting that the change in geometry resulted in these samples undergoing a separate (but to all appearances identical) sinter cycle to all other samples.

Figure 7 presents both numerical and morphological analyses of the surface roughness. The main contributors to the roughness are the extrusion of tracks and layers. The surface roughness values depicted in Figs. 7 and 6 were obtained from the free surface, opposite to the side where the support structure is attached to the sample. It is important to note that these values are not consistently similar around the circumference of the round samples.

For example, on the side of the samples (built at 30°), the surface roughness measured approximately 9.56 µm, whereas the top surface and the bottom surface (support structure side) exhibited roughness values of 14.23 µm and 18.10 µm, respectively, which are significantly higher. However, the vertically built samples do not have a support structure, resulting in more consistent roughness values around the circumference of the samples, averaging at 10.22 µm. The only exception is the joining line of the extruded tracks, which exhibits a roughness value of 16.5 µm but appears as a much thinner line along the length of the sample.

The roughness values displayed in Fig. 7 are consistent with those in Fig. 6. However, it is important to clarify that these values represent the average of three measurements, which were taken randomly along the longitudinal direction of the samples.

Furthermore, the observed low UTS values of samples built at 30° and 60° can be partially attributed to the high surface roughness values on the side and bottom side (support structure side) of the samples.

3.2 Relative density and porosity observed

Figure 8a illustrates the relative density of samples with various orientations. These as-built samples were subjected to Archimedes' density measurement according to ASTM B962, and each sample was measured three times. The average density of all as-built samples was found to be very similar, except for those with a 60° orientation. However, the heat-treated samples exhibited a slightly higher density, reaching approximately 96%. This suggests that the heat treatment process has the potential to improve the density of the samples by aiding in the closure of voids remaining after the sintering process.

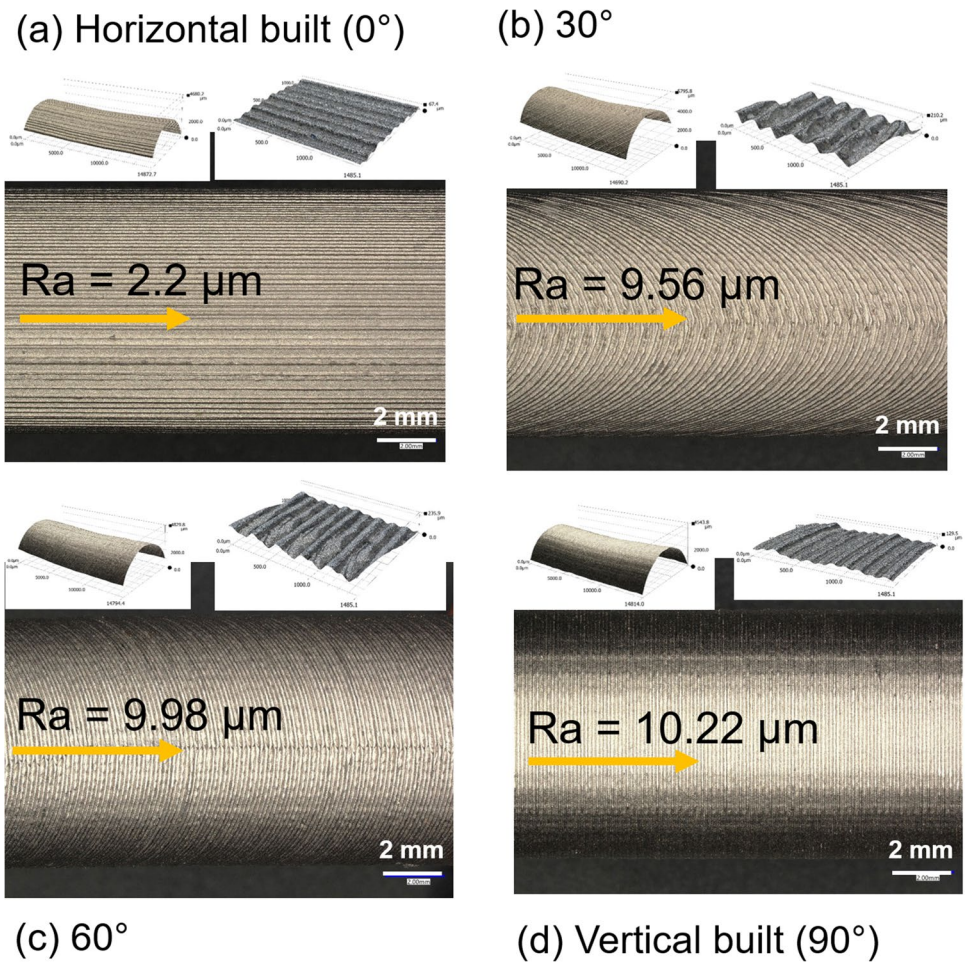

Fig. 7 Optical images show the as-built sample in various orientations. **a** Built along the horizontal orientation. **b** Built at 30° orientation. **c** Built at 60° orientation. **d** Built in the vertical orientation. Arrows indicate the direction of surface roughness measurement using the Talysurf stylus. The extrude print track is presented as straight (0°), curved (30° and 60°), and vertical (90°).

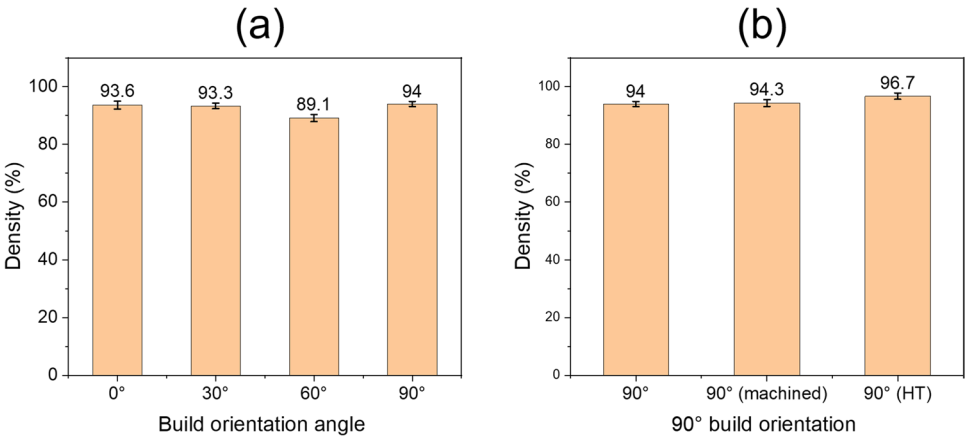

Fig. 8 The average relative density of as-built samples with different orientations (**a**), and 90° (vertical) sample density as-built, machined, and after H900 heat treatment (**b**)

Images of the porosity observed by SEM is shown in Fig. 9. These images offer visual evidence that supports the density findings, as they reveal a high occurrence of porosities in the cross section. SEM analysis focused on a sample with a 0° orientation, demonstrating the presence of porosities ranging in size from 250 to 1 µm.

3.3 Fracture surface analysis

SEM analysis of fractured surfaces from various orientations revealed similar failure mechanisms in all orientation specimens. Fracture occurred at the interface between layers deposited to build the part or tracks of extruded

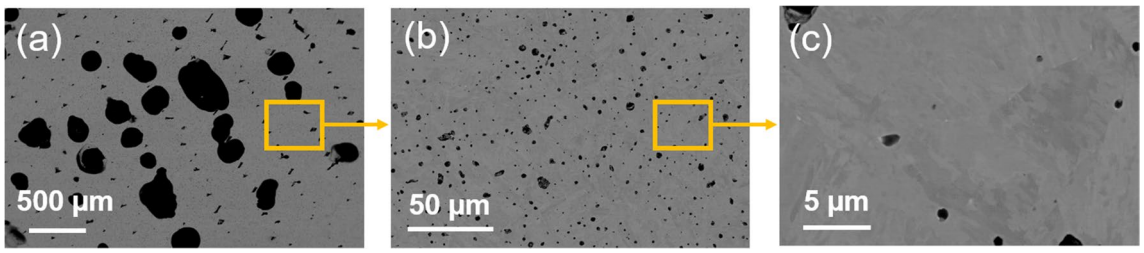

Fig. 9 The SEM microstructure at various magnifications (**a** to **c**) illustrates the distribution of pores within the build, ranging from 250 to 1 µm

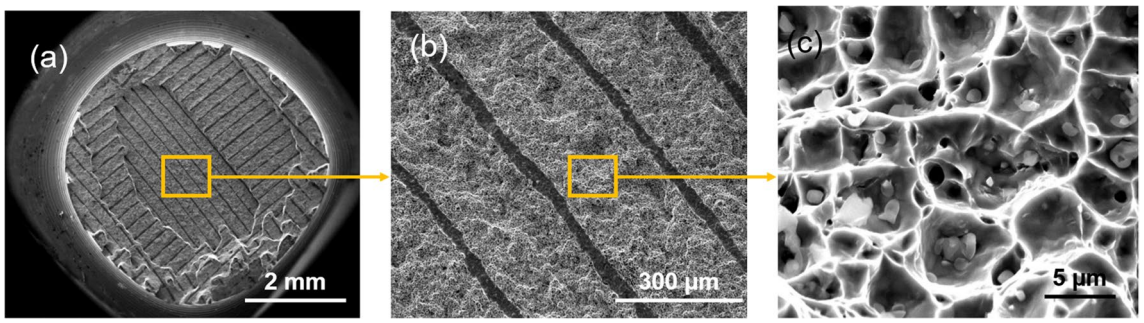

Fig. 10 SEM analysis of the fracture surface illustrating microstructural features and characteristics, indicating brittle failure caused by incomplete closure of filament roads and the presence of loose particles

material. Fig. 10a illustrates the brittle fracture behaviour observed on the fractured surface of the vertically built sample, showing limited evidence of plastic deformation. This indicates that the material experienced minimal deformation before fracturing, suggesting low energy absorption during the tensile loading process.

Figure 10b shows individual filament roads that were not fully overlapped, resulting in visible gaps between each road. This observation suggests inadequate adhesion between the deposited filaments during the sintering process, leading to incomplete fusion of the material. The presence of voids and loose particles within the internal structure of the parts, as depicted in Fig. 10c, further supports this finding. These gaps, voids, and loose particles contribute to the observed brittle fracture behaviour and limited plastic deformation during tensile testing.

EDS analysis in Fig. 11 reveals that the loose particles within the material's pores primarily consist of Cr, Fe, and Si elements, which are typical constituents of the 17-4PH stainless steel used in the printing. The presence of these particles within the pores indicates incomplete fusion or bonding with the surrounding material during the sintering process. The detection of oxygen in the EDS analysis could be attributed to the presence of oxygen in the ambient air during the analysis or to chemical reactions between the loose particles and the surrounding environment during sintering.

4 Discussion

This study has demonstrated here that there are significant differences in the as-built tensile performance of MetalX^{TM} components with orientation (i.e. anisotropy). This collaborates previously published research by other authors [16, 21, 23–25]. However, post-built machining helps to both increase the absolute UTS and improve the isotropy of the material. Further improvements are possible by heat treatment.

However, all the samples showed low ductility. We attribute this to the large pores, along with surface roughness, observed. Specifically, the presence of porosity and surface roughness contributes to a brittle failure mode rather than a ductile failure mode for all the samples.

The variation observed in the as-built UTS with orientation, as noted in this study, exhibits a similar trend to that reported in previous literature (Table 1 and Fig. 12). However, notable differences in absolute values are observed. All studies have noted a higher UTS in the horizontal orientation than the vertical orientation. Additionally, Alkindi et al. [31], similar to the findings presented in this study, identified a decline in ultimate tensile strength (UTS) as the orientation transitioned from 0 to 30° and subsequently to 60° (reaching its lowest point), followed by an increase at 90°. The observed anisotropy thus emerges as a shared

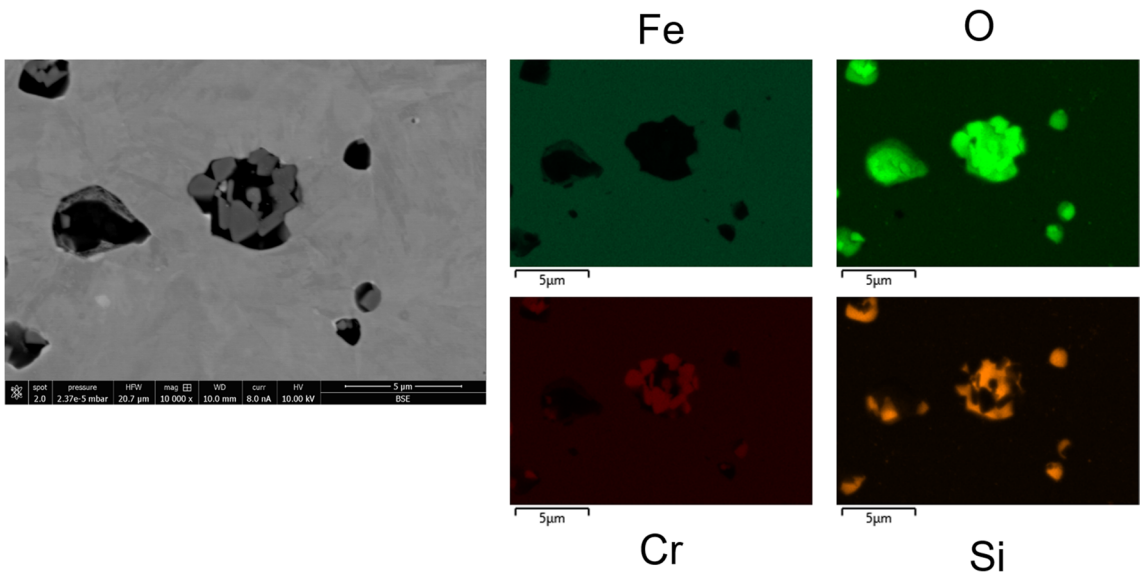

Fig. 11 EDS analysis of the sintered sample revealing the presence of particles containing Fe, Cr, and Si, along with O_2

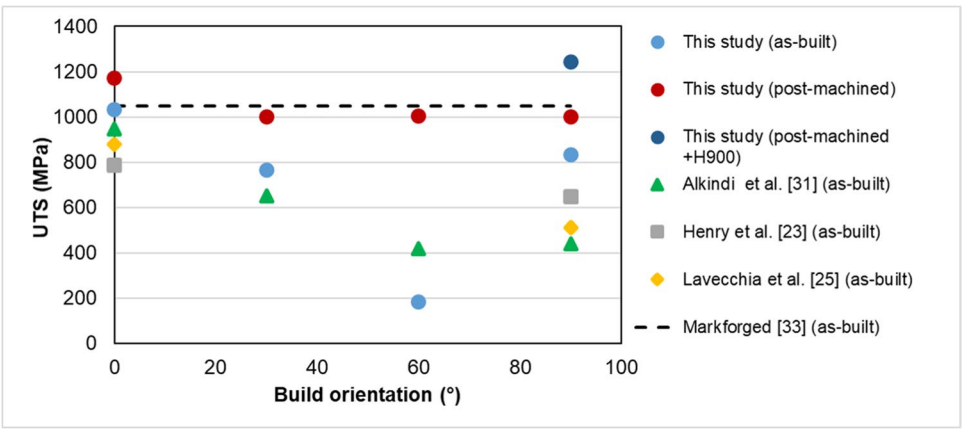

Fig. 12 Effect of orientation on UTS, data from this study, and previous works

characteristic across various studies, suggesting that it is induced by the manufacturing process. While the ADAM process parameters are not disclosed by Markforged, the end user has the flexibility to define the number of outer layers. In the study conducted by Lavecchia et al. [25], the specified number of outer wall layers is six, whereas in the study by Alkindi et al. [31], it is four. However, the study conducted by Henry et al. [23] does not provide information regarding the number of layers.

The average UTS of horizontally built parts was 1035 MPa, a figure comparable to both metal injection molding (MIM) values (950–1050 MPa) and wrought values (1000–1050 MPa) for 17-4PH stainless steel [35]. The recorded as-built UTS values were generally higher than those previously published, with only one exception. However, all data were below the Markforged quoted value of 1050 MPa. Discrepancies between various studies cannot be easily explained. However, one issue of concern is the black box nature of the sintering cycle. The exact temperature and times are unknown and set by Markforged, which could lead to differences to the furnace program without user knowledge. It has been observed that the hardness of a specimen produced in a distinct sintering cycle was noticeably elevated, and no apparent reasons for this discrepancy were identified. It is therefore possible that different studies unknowingly used different sinter cycles. This is of great concern should industry wish to certify the material for a critical application.

After machining, the data for the 0° orientation indicated that the UTS was above the value quoted by Markforged, while other orientations remained consistently around 1000 MPa. This suggests that the average machined UTS aligns with the values provided by Markforged. However, this overlooks the high levels of anisotropy, which must be

considered when designing components to be manufactured by this method.

Similarly, the vertically built, machined, and H900 heat-treated sample exhibited a value close to, but slightly below, the figure stated by Markforged, with an observed UTS of 1242 MPa against the stated 1250 MPa. It appears plausible that if horizontally machined samples were tested in the heat-treated condition, their UTS would likely be higher. The heat treatment was also observed to marginally improve the measured density, a factor that may contribute to enhanced fatigue performance of the material [36]. Consequently, these findings indicate the potential of heat treatment as a valuable post-processing step for augmenting the overall quality of the final ADAM-fabricated product.

Two potential reasons account for the enhanced performance after machining: the substantial reduction in surface roughness and the removal of the outer walls initially deposited during the FFF process, allowing for the evaluation of the infill material exclusively.

Considering first the removal of the outer walls. Leonard and Tammas-Williams [26] showed that there was a periodic layer wise gap between the walls and the infill after printing that failed to heal during sintering. This gap was present at the top and bottom of each layer. Removal of this gap by machining, and the associated increase in density, is likely to contribute to the increase in the UTS. Nevertheless, it is essential to highlight that the density measurements conducted in this study revealed no significant increase in relative density after machining. This lack of change may be attributed to the fact that all measurements were taken on planes that did not intersect with the voids observed by Leonard, which were exclusively present at the top and bottom of each layer.

Considering next the surface roughness of the vertical orientated specimens, it was observed that as the surface roughness decreased in the vertical as-built, machined, and polished conditions respectively, the UTS increased (Fig. 6b). This suggests that improving the surface finish of the material can effectively reduce stress concentrations and improve components overall strength. Similar effects have been observed in other metal AM processes, e.g. PBF of stainless steel [37].

Thus, the results shown in Fig. 6 suggest that improving the surface finish of the parts through post-processing methods such as machining, polishing, and heat treatment with post-machining can increase their UTS. Therefore, it is important to consider post-processing as a critical step in the production of metal 3D printed parts to ensure that they meet the required mechanical properties for their intended applications.

The most significant post-machining improvements in UTS were observed in the parts built at 30° and 60° orientations. In particular, the 60° orientation showed a fourfold improvement in UTS after machining. The surface roughness of angled (i.e. not 0° or 90° to build direction) FFF parts is often dominated by the 'staircase effect' [38] caused by the layer-by-layer deposition process inherent to FFF. The staircase effect arises from the layer-by-layer deposition of material during the FFF process, as depicted in Fig 7, with periodic variations corresponding to the layer thickness (100 µm) after sintering. The stress concentrations introduced by these steps may explain why as-built samples tested at 30° and 60° orientations exhibit lower strength compared to those at 0° or 90° orientations. When the as-built surface is removed, the samples orientated at 30°, 60°, and 90° showed very similar UTS.

It can also be hypothesised that improvements in the tensile properties of the material may be achieved through the minimization of roughness by adjusting the material deposition parameters. This may involve optimising parameters such as layer thickness, printing speed, and temperature to achieve a smoother surface finish [39]. By fine-tuning these parameters, it is possible to mitigate the roughness and perhaps improve the overall quality of the printed material.

Following machining, the UTS values for the 0°, 30°, and 60° orientations exhibited similarities. However, the 0° orientation showed a notable difference after machining. Fractography analysis revealed that the other orientations failed at the interface between layers. Notably, local stress was elevated at the interface due to the presence of aligned voids between deposited extrudes. The substantial voids observed on the fracture surface (Fig. 10) of the components may have originated from inadequate overlap between extrusion tracks during material deposition. The orientation of the voids on the fracture surface varied based on the orientation used in the FFF process. These voids within the internal structure of the components contributed to their failure at the layer interface, potentially contributing to the observed limited ductility across all samples.

Conversely, at 0°, there was minimal stress perpendicular to the layers, and the machined sample exhibited the highest UTS among those tested. This finding underscores the possibility of enhancing the properties of the MetalX^{TM} material through modifications to the FFF process.

5 Conclusions

In conclusion, the evaluation of tensile properties in 17-4PH stainless steel samples produced through the ADAM process underscores the significant impact of surface finish and post-processing on material characteristics. Variations in properties are attributed primarily to surface roughness introduced during the initial FFF deposition phase and the presence of substantial voids, likely occurring during FFF. The study reveals inconsistencies in hardness among

nominally identical samples subjected to different sintering cycles, raising concerns about the undisclosed nature of the sinter cycle and its potential influence on part temperatures.

The main findings are summarised as below.

- Considering as-built samples, the highest UTS values were obtained from horizontally oriented samples, reaching 1034.5 MPa. In comparison, UTS values for other orientations—30°, 60°, and 90°—were 764.7 MPa, 183.5 MPa, and 831.7 MPa, respectively
- The post-processing methods, encompassing machining, polishing, and heat treatment, play a pivotal role in enhancing the UTS. The UTS after machining averages around 1000 MPa across various orientations (30°, 60°, and 90°). Particularly noteworthy is the significant improvement observed at the 30° orientation, increasing from 764.7 to 1001 MPa, and at the 60° orientation, surging from 183.5 MPa to 1005 MPa, indicating a notable fourfold increase at 60°. This underscores that machining not only enhances absolute UTS but also contributes to achieving material isotropy.
- Furthermore, the application of heat treatment results in a further elevation of UTS and density, establishing itself as a valuable post-processing step. Specifically, machined and heat-treated vertically printed samples exhibit even higher UTS values, reaching 1242 MPa, in stark contrast to the as-built samples with a UTS value of 831.7 MPa. This compelling improvement demonstrates the synergistic effect of machining and heat treatment, showcasing their potential for significantly enhancing the mechanical properties of the material.
- The correlation between decreasing surface roughness and increased UTS highlights the critical role of surface finish. Process parameter optimization to minimise roughness emerges as a potential avenue for enhancing tensile properties. The identified 'staircase effect' in angled FFF parts, particularly at 30° and 60° orientations, contributes to reduced strength.
- The overall observation of low ductility in all samples, attributed to large pores and surface roughness, underscores the prevalence of a brittle failure mode. This understanding reinforces the need for careful consideration of post-processing steps to address these inherent material characteristics. The lack of transparency in the sintering cycle raises concerns about consistent material properties and suggests a critical need for enhanced process control and traceability in additive manufacturing systems.

In summary, while the ADAM metal FFF process provides a cost-effective avenue for metal additive manufacturing, this study underscores the importance of comprehending and controlling printing and sintering process parameters to achieve desired material properties. The results highlight potential inconsistencies in material properties, emphasizing the necessity of post-processing to attain the desired mechanical characteristics. Encouragingly, the reduction in anisotropy after machining signals an avenue for improving material performance, reinforcing the importance of post-processing in achieving reliable and consistent outcomes.

Acknowledgements The authors would like to express their gratitude to Thomas Byrne, Clive Eyre, Richard Dodd, and Mohammed Radwani for their valuable assistance in conducting the experiments.

Author contribution All authors contributed to the study conception and design. Material preparation, data collection, and analysis were performed by Tahsin Opoz, Hiren Kotadia, and Juan Ahuir-Torres. The first draft of the manuscript was written by Tahsin Opoz and Andrew Burgess, Sam Tammas-Williams, and all authors commented on previous versions of the manuscript. All authors read and approved the final manuscript.

Declarations

Competing interests The authors declare no competing interests.

References

1. Frazier WE (2014) Metal additive manufacturing: a review. J Mater Eng Perform 23:1917–1928. https://doi.org/10.1007/s11665-014-0958-z
2. Sames WJ, List FA, Pannala S, Dehoff RR, Babu SS (2016) The metallurgy and processing science of metal additive manufacturing. Int Mater Rev 61:315–360. https://doi.org/10.1080/09506608.2015.1116649
3. Kotadia HR, Gibbons G, Das A, Howes PD (2021) A review of laser powder bed fusion additive manufacturing of aluminium alloys: microstructure and properties. Addit Manuf 46:102155. https://doi.org/10.1016/j.addma.2021.102155
4. Aslan B, Yıldız AR (2020) Optimum design of automobile components using lattice structures for additive manufacturing. Mater Test 62:633–639. https://doi.org/10.3139/120.111527
5. Kopar M, Yildiz AR (2023) Experimental investigation of mechanical properties of PLA, ABS, and PETG 3-d printing materials using fused deposition modeling technique. Mater Test 65:1795–1804. https://doi.org/10.1515/mt-2023-0202
6. Ngo TD, Kashani A, Imbalzano G, Nguyen KTQ, Hui D (2018) Additive manufacturing (3D printing): a review of materials, methods, applications and challenges. Compos Part B: Eng 143:172–196. https://doi.org/10.1016/j.compositesb.2018.02.012

7. Brennan MC, Keist JS, Palmer TA (2021) Defects in metal additive manufacturing processes. J Mater Eng Perform 30:4808–4818. https://doi.org/10.1007/s11665-021-05919-6
8. Kumar M, Gibbons GJ, Das A, Manna I, Tanner D, Kotadia HR (2021) Additive manufacturing of aluminium alloy 2024 by laser powder bed fusion: microstructural evolution, defects and mechanical properties. Rapid Prototyp J 27:1388–1397. https://doi.org/10.1108/RPJ-10-2020-0241
9. Pérez-Ruiz JD, de Lacalle LNL, Urbikain G, Pereira O, Martínez S, Bris J (2021) On the relationship between cutting forces and anisotropy features in the milling of LPBF Inconel 718 for near net shape parts. Int J Mach Tools Manuf 170:103801. https://doi.org/10.1016/j.ijmachtools.2021.103801
10. Pérez-Ruiz J, González-Barrio H, Sanz-Calle M, Gómez-Escudero G, Munoa J, de Lacalle LL (2023) Machining stability improvement in LPBF printed components through stiffening by crystallographic texture control. CIRP Annals 72:141–144. https://doi.org/10.1016/j.cirp.2023.03.025
11. Gibson I, Rosen DW, Stucker B, Khorasani M, Rosen D, Stucker B, Khorasani M (2021) Additive manufacturing technologies, 3rd edn. Springer
12. Horn TJ, Harrysson OLA (2012) Overview of current additive manufacturing technologies and selected applications. Sci Prog 95:255–282. https://doi.org/10.3184/003685012X13420984463047
13. Guo N, Leu MC (2013) Additive manufacturing: technology, applications and research needs. Front Mech Eng 8:215–243. https://doi.org/10.1007/s11465-013-0248-8
14. Tan JH, Wong WLE, Dalgarno KW (2017) An overview of powder granulometry on feedstock and part performance in the selective laser melting process. Addit Manuf 18:228–255. https://doi.org/10.1016/j.addma.2017.10.011
15. Anderson IE, White EM, Dehoff R (2018) Feedstock powder processing research needs for additive manufacturing development. Curr Opin Solid State Mater Sci 22:8–15
16. Suwanpreecha C, Seensattayawong P, Vadhanakovint V, Manonukul A (2021) Influence of specimen layout on 17-4PH (AISI 630) alloys fabricated by low-cost additive manufacturing. Metall Mater Trans A 52:1999–2009. https://doi.org/10.1007/s11661-021-06211-x
17. Roth GA, Geraci CL, Stefaniak A, Murashov V, Howard J (2019) Potential occupational hazards of additive manufacturing. J Occup Environ Hyg 16:321–328. https://doi.org/10.1080/15459624.2019.1591627
18. Rejeski D, Zhao F, Huang Y (2018) Research needs and recommendations on environmental implications of additive manufacturing. Addit Manuf 19:21–28. https://doi.org/10.1016/j.addma.2017.10.019
19. Singh S, Singh G, Prakash C, Ramakrishna S (2020) Current status and future directions of fused filament fabrication. J Manuf Process 55:288–306. https://doi.org/10.1016/j.jmapro.2020.04.049
20. Gao C, Wolff S, Wang S (2021) Eco-friendly additive manufacturing of metals: energy efficiency and life cycle analysis. J Manuf Syst 60:459–472. https://doi.org/10.1016/j.jmsy.2021.06.011
21. Cañadilla A, Romero A, Rodríguez GP, Caminero MÁ, Dura ÓJ (2022) Mechanical, electrical, and thermal characterization of pure copper parts manufactured via material extrusion additive manufacturing. Materials 15:4644
22. Parenti P, Puccio D, Colosimo BM, Semeraro Q (2022) A new solution for assessing the printability of 17-4 PH gyroids produced via extrusion-based metal AM. J Manuf Process 74:557–572. https://doi.org/10.1016/j.jmapro.2021.12.043
23. Henry TC, Morales MA, Cole DP, Shumeyko CM, Riddick JC (2021) Mechanical behavior of 17-4 PH stainless steel processed by atomic diffusion additive manufacturing. Int J Adv Manuf Technol 114:2103–2114. https://doi.org/10.1007/s00170-021-06785-1
24. Pellegrini A, Palmieri ME, Guerra MG (2022) Evaluation of anisotropic mechanical behaviour of 316L parts realized by metal fused filament fabrication using digital image correlation. Int J Adv Manuf Technol 120:7951–7965. https://doi.org/10.1007/s00170-022-09303-z
25. Lavecchia F, Pellegrini A, Galantucci LM (2023) Comparative study on the properties of 17-4 PH stainless steel parts made by metal fused filament fabrication process and atomic diffusion additive manufacturing. Rapid Prototyp J 29:393–407. https://doi.org/10.1108/RPJ-12-2021-0350
26. Léonard F, Tammas-Williams S (2022) Metal FFF sintering shrinkage rate measurements by X-ray computed tomography. Nondestruct Test Eval 37:631–644. https://doi.org/10.1080/10589759.2022.2085702
27. Jiang D, Ning F (2022) Physical-mechanical behaviors of stainless steel plate-lattice built by material extrusion additive manufacturing. J Mater Process Technol 309:117739. https://doi.org/10.1016/j.jmatprotec.2022.117739
28. Gonzalez-Gutierrez J, Cano S, Schuschnigg S, Kukla C, Sapkota J, Holzer C (2018) Additive manufacturing of metallic and ceramic components by the material extrusion of highly-filled polymers: a review and future perspectives. Materials 11:840
29. Galati M, Minetola P (2019) Analysis of density, roughness, and accuracy of the atomic diffusion additive manufacturing (ADAM) process for metal parts. Materials 12:4122
30. Günaydın AC, Yıldız AR, Kaya N (2022) Multi-objective optimization of build orientation considering support structure volume and build time in laser powder bed fusion. Mater Test 64:323–338. https://doi.org/10.1515/mt-2021-2075
31. Alkindi T, Alyammahi M, Susantyoko RA, Atatreh S (2021) The effect of varying specimens' printing angles to the bed surface on the tensile strength of 3D-printed 17-4PH stainless-steels via metal FFF additive manufacturing. MRS Commun 11:310–316. https://doi.org/10.1557/s43579-021-00040-0
32. Tosto C, Tirillò J, Sarasini F, Cicala G (2021) Hybrid metal/polymer filaments for fused filament fabrication (FFF) to print metal parts. Appl Sci 11. https://doi.org/10.3390/app11041444
33. Material Datasheet 17-4 PH stainless steel (2018) https://markforged.com/datasheets. [REV 2.0 - 7/25/2018]. Available from: https://static.markforged.com/downloads/markforged_datasheet_17-4_ph_stainless_steel.pdf. Accessed 20 May 2023
34. Gerosa R, Rivolta B, Sala A (2008) Optimization of the heat treatment of a 17-4 PH stainless steel by dilatometric technique. J ASTM Int 5:JAI101779. https://doi.org/10.1520/JAI101779
35. Irrinki H, Jangam JSD, Pasebani S, Badwe S, Stitzel J, Kate K, Gulsoy O, Atre SV (2018) Effects of particle characteristics on the microstructure and mechanical properties of 17-4 PH stainless steel fabricated by laser-powder bed fusion. Powder Technol 331:192–203. https://doi.org/10.1016/j.powtec.2018.03.025
36. Aboulkhair NT, Maskery I, Tuck C, Ashcroft I, Everitt NM (2016) Improving the fatigue behaviour of a selectively laser melted aluminium alloy: influence of heat treatment and surface quality. Mater Design 104:174–182. https://doi.org/10.1016/j.matdes.2016.05.041
37. Afkhami S, Dabiri M, Piili H, Björk T (2021) Effects of manufacturing parameters and mechanical post-processing on stainless steel 316L processed by laser powder bed fusion. Mater Sci Eng: A 802:140660. https://doi.org/10.1016/j.msea.2020.140660
38. Angelo LD, Stefano PD, Marzola A (2017) Surface quality prediction in FDM additive manufacturing. Int J Adv Manuf Technol 93:3655–3662. https://doi.org/10.1007/s00170-017-0763-6
39. Turner BN, Gold SA (2015) A review of melt extrusion additive manufacturing processes: II. Materials, dimensional accuracy, and surface roughness. Rapid Prototyp J 21:250–261. https://doi.org/10.1108/RPJ-02-2013-0017